JHEP

Published for SISSA by Springer

Received: June 20, 2014
Revised: October 8, 2014
Accepted: November 8, 2014
Published: November 26, 2014

JHEP11(2014)149

A refined holographic QCD model and QCD phase structure

Yi Yang[a,b] **and Pei-Hung Yuan**[c]

[a] *Department of Electrophysics, National Chiao Tung University, 1001 University Street, Hsinchu, R.O.C.*

[b] *National Center for Theoretical Sciences, 1001 University Street, Hsinchu, R.O.C.*

[c] *Institute of Physics, National Chiao Tung University, 1001 University Street, Hsinchu, R.O.C.*

E-mail: yiyang@mail.nctu.edu.tw, phy.pro.phy@gmail.com

Abstract: We consider the Einstein-Maxwell-dilaton system with an arbitrary kinetic gauge function and a dilaton potential. A family of analytic solutions is obtained by the potential reconstruction method. We then study its holographic dual QCD model. After fixing the kinetic gauge function by requesting the linear Regge spectrum of mesons, we calculate the free energy to obtain the phase diagram of the holographic QCD model.

Keywords: Gauge-gravity correspondence, Phase Diagram of QCD

ArXiv ePrint: 1406.1865

doi:10.1007/JHEP11(2014)149

Contents

1 Introduction

Studying phase structure in QCD theory is an important and challenging task. It is well known that QCD is in the confinement and chiral symmetry breaking phase at low temperature/density, while it is in the deconfinement and chiral symmetry restored phase at high temperature/density. It is widely believed that there exists a phase transition between these two phases. To obtain the phase transition boundary in the $T-\mu$ phase diagram is a rather difficult task since the QCD coupling constant becomes very strong near the phase transition region and the conventional perturbative method does not work at all. Moreover, with the nonzero physical quark masses presented, part of the phase transition line will weaken to a crossover for a range of temperature and chemical potential that makes the phase structure of QCD more complicated. Locating the critical point where the phase transition converts to a crossover is a crucial but rather difficult task. For a long time, the technique of lattice QCD is the only reliable method to attack these problems. Although lattice QCD works very well for zero density, it encounters the sign problem when considering finite density or chemical potential, i.e. $\mu \neq 0$. However, the most interesting region in the QCD phase diagram is at finite density. The most concerned subjects, such as heavy-ion collisions and compact stars in astrophysics, are all related to QCD at finite density. Recently, lattice QCD has developed some techniques to solve the sign problem, such as reweighting method, imaginary chemical potential method and the method of expansion in μ/T etc. Nevertheless, these techniques are only able to deal with the cases of small chemical potentials and quickly lost control for the larger chemical potential. See [1] for a review of the current status of lattice QCD.

On the other hand, using the recently developed idea of AdS/CFT correspondence from string theory, one is able to study QCD in the strongly coupled region by studying its weakly coupled dual gravitational theory, so called holographic QCD. Briefly speaking, there are two types of holographic QCD models, i.e. top-down and bottom up models. The models which are directly constructed from string theory are called top-down models.

JHEP11(2014)149

The most popular top-down models are D3-D7 [2–5] model and D4-D8 (Sakai-Sugimoto) model [6, 7]. In these top-down holographic QCD models, confinement and chiral symmetry phase transitions in QCD have been addressed and translated into geometric transformations in the dual gravity theories. Meson spectrums and their decay constants have also been calculated and compared with the experimental data with surprisingly consistency. Although the top-down QCD models describe many important properties in realistic QCD, the meson spectrums obtained from those models can not realize the linear Regge trajectories. To solve this problem, another type of holographic models have been developed, i.e. bottom-up models, such as the hard wall model [8] and the later refined soft-wall model [9]. In the original soft-wall model, the IR correction of the dilaton field was put by hand to obtain the linear Regge behavior of the meson spectrum. However, since the fields configuration is put by hand, it does not satisfy the equations of motion. To get a fields configuration which is both consistent with the equation of motions and realizes the linear Regge trajectory, dynamical soft-wall models were constructed by introduce a dilaton potential consistently [10, 11]. On the other hand, the Einstein-dilaton and Einstein-Maxwell-dilaton models have been widely studied numerically [12–16] to investigate the thermodynamical properties and explore the phase structure in QCD. Recently, by the potential reconstruction method, analytic solutions have been obtained in the Einstein-dilaton model [17] as well as in the Einstein-Maxwell-dilaton model [16, 18].

In this paper, we try to combine the techniques of the dynamical soft-wall model and the potential reconstruction methods to study both QCD phase diagram and the linear Regge spectrum of mesons in a single model. We consider an Einstein-Maxwell-dilaton system with an arbitrary kinetic gauge function and a dilaton potential as in [19]. A family of analytic solutions are obtained by the potential reconstruction method. We then study its holographic dual QCD model. The linear Regge trajectories of meson spectrums can be realized by choosing an appropriate kinetic gauge function. By studying the thermodynamics of the Einstein-Maxwell-dilaton background, we calculate the free energy to obtain the phase diagram of our holographic QCD model. We compute the different equation of states in our model and discuss their characters.

The paper is organized as follows. In section 2, we consider the Einstein-Maxwell-dilaton system with a dilaton potential and a gauge kinetic function. By potential reconstruction method, we obtain a family of analytic solutions with arbitrary gauge kinetic function and warped factor. We then fix the gauge kinetic function by requesting the meson spectrums to realize the linear Regge trajectories. By choosing an appropriate warped factor, we obtain the final form of our analytic solution. In section 3, we study the thermodynamics of our gravitational background and compute the free energy to get the phase diagram of QCD. We summary and discuss our result in section 4.

2 Einstein-Maxwell-Dilaton system

We consider a 5-dimensional Einstein-Maxwell-dilaton system with probe flavor fields as in [19]. The action of the system have two parts, the background part and the matter part,

$$S = S_b + S_m. \tag{2.1}$$

JHEP11(2014)149

The background action includes a gravity field $g_{\mu\nu}$, a Maxwell field A_μ and a neutral dilatonic scalar field ϕ. The matter action includes two flavor fields $\left(A_\mu^L, A_\mu^R\right)$, representing the left-handed and right-handed gauge fields, respectively. The Kaluza-Klein modes of these 5d flavor gauge fields describe the degrees of freedom of mesons on the 4d boundary. We will treat the matter fields as probe fields and do not consider their backreaction to the background.

In Einstein frame, the background action and the matter action can be written as

$$S_b = \frac{1}{16\pi G_5}\int d^5x\sqrt{-g}\left[R - \frac{f\left(\phi\right)}{4}F^2 - \frac{1}{2}\partial_\mu\phi\partial^\mu\phi - V\left(\phi\right)\right], \tag{2.2}$$

$$S_m = -\frac{1}{16\pi G_5}\int d^5x\sqrt{-g}\frac{f\left(\phi\right)}{4}\left(F_V^2 + F_{\tilde{V}}^2\right), \tag{2.3}$$

where $f\left(\phi\right)$ is the gauge kinetic function and $V\left(\phi\right)$ dilaton potential. Moreover, we have expressed the flavor fields A^L and A^R in terms of the vector meson field and pseudovector meson field V and $\tilde{V}$,

$$A^L = V + \tilde{V}, \qquad A^R = V - \tilde{V}. \tag{2.4}$$

The equations of motion can be derived from the actions (2.2) and (2.3),

$$\nabla^2\phi = \frac{\partial V}{\partial\phi} + \frac{1}{4}\frac{\partial f}{\partial\phi}\left(F^2 + F_V^2 + F_{\tilde{V}}^2\right), \tag{2.5}$$

$$\nabla_\mu\left[f(\phi)F^{\mu\nu}\right] = 0, \tag{2.6}$$

$$\nabla_\mu\left[f(\phi)F_V^{\mu\nu}\right] = 0, \tag{2.7}$$

$$\nabla_\mu\left[f(\phi)F_{\tilde{V}}^{\mu\nu}\right] = 0, \tag{2.8}$$

$$R_{\mu\nu} - \frac{1}{2}g_{\mu\nu}R = \frac{f(\phi)}{2}\left(F_{\mu\rho}F_\nu^\rho - \frac{1}{4}g_{\mu\nu}F^2 + \left\{F_V, F_{\tilde{V}}\right\}\right) + \frac{1}{2}\left[\partial_\mu\phi\partial_\nu\phi - \frac{1}{2}g_{\mu\nu}\left(\partial\phi\right)^2 - g_{\mu\nu}V\right]. \tag{2.9}$$

First, we will solve the gravitational background in the above Einstein-Maxwell-dilaton system. We consider the following ansatz for the metric, the Maxwell field and the dilaton field,

$$ds^2 = \frac{L^2e^{2A(z)}}{z^2}\left[-g(z)dt^2 + \frac{dz^2}{g(z)} + d\vec{x}^2\right], \tag{2.10}$$

$$\phi = \phi\left(z\right), \qquad A_\mu = A_t\left(z\right), \tag{2.11}$$

where $z = 0$ corresponds to the conformal boundary of the 5d spacetime and we will set the radial L of AdS_5 space to be unit in the following of this paper. By turning off the probe fields V and $\tilde{V}$ in eqs. (2.5)–(2.9), the equations of motion for the background fields become

$$\phi'' + \left(\frac{g'}{g} + 3A' - \frac{3}{z}\right)\phi' + \left(\frac{z^2e^{-2A}A_t'^2f_\phi}{2g} - \frac{e^{2A}V_\phi}{z^2g}\right) = 0, \tag{2.12}$$

$$A_t'' + \left(\frac{f'}{f} + A' - \frac{1}{z}\right)A_t' = 0, \tag{2.13}$$

JHEP11(2014)149

$$A'' - A'^2 + \frac{2}{z}A' + \frac{\phi'^2}{6} = 0, \tag{2.14}$$

$$g'' + \left(3A' - \frac{3}{z}\right)g' - e^{-2A}z^2 f A_t'^2 = 0, \tag{2.15}$$

$$A'' + 3A'^2 + \left(\frac{3g'}{2g} - \frac{6}{z}\right)A' - \frac{1}{z}\left(\frac{3g'}{2g} - \frac{4}{z}\right) + \frac{g''}{6g} + \frac{e^{2A}V}{3z^2 g} = 0. \tag{2.16}$$

We should notice that only four of the above five equations are independent. In the following, we will solve the equations (2.13)–(2.16), and leave the equation (2.12) as a constraint for the consistent check.

We impose the regular boundary conditions at the horizon $z = z_{\mathrm{H}}$ and the asymptotic AdS condition at the boundary $z \to 0$ as follows,

$$A_t(z_{\mathrm{H}}) = g(z_{\mathrm{H}}) = 0, \tag{2.17}$$

$$A(0) = -\sqrt{\frac{1}{6}}\phi(0), \qquad g(0) = 1, \tag{2.18}$$

where the condition (2.17) ensures that $A_\mu A^\mu = g^{tt}A_0 A_0$ is finite at $z = z_{\mathrm{H}}$, and the condition (2.18) guarantees that the metric is asymptotic to an AdS spacetime at $z \to 0$. Furthermore, at $z \to 0$, the gauge field can be expanded as

$$A_t(0) = \mu + \rho z^2 + \cdots, \tag{2.19}$$

where μ is quark chemical potential and ρ is quark density.

Now, we are ready to solve the eqs. (2.13)–(2.16) with the boundary conditions (2.17), (2.18). We are going to solve the equations by using the so called potential reconstruction method. In this method, we regard the field $A(z)$ as a given function but treat the potential $V(\phi)$ as an unknown function to be solved consistently with other fields. Since $\phi(z)$ is a function of z, we can treat the gauge kinetic function $f(\phi)$ and the dilaton potential $V(\phi)$ as functions of z, i.e. $f(z)$ and $V(z)$, when we solve the equations of motion. In summary, we will solve the fields $\{\phi(z), A_t(z), g(z), V(z)\}$ in terms of two given functions $\{f(z), A(z)\}$.

We start from eq. (2.14), which is easy to be solved as

$$\phi'(z) = \sqrt{-6\left(A'' - A'^2 + \frac{2}{z}A'\right)}, \tag{2.20}$$

provided we regard the field $A(z)$ as a given function. Next, $A_t(z)$ can be solved from eq. (2.13),

$$A_t(z) = C_{A_t}\int_{z_{\mathrm{H}}}^{z} \frac{y}{e^{A(y)}f(y)}dy, \tag{2.21}$$

where C_{A_t} is an integral constant and we have used the boundary condition $A_t(z_{\mathrm{H}}) = 0$ to fix the other integral constant, the lower limit of the integral, to be z_{H}. Plug eq. (2.21) into eq. (2.15), we can solve $g(z)$ as

$$g(z) = 1 + C_{A_t}^2\int_0^z y^3 e^{-3A(y)}dy\int_{y_g}^{y}\frac{x}{e^{A(x)}f(x)}dx, \tag{2.22}$$

JHEP11(2014)149

where y_g is another integral constant and we have used the boundary condition $g(0)=1$ to fix the lower limit of the integral for y to be 0. Now we can use the boundary condition $g(z_{\rm H})=0$ to fix the constant C_{A_t} as

$$C_{A_t}=\sqrt{\frac{-1}{\int_0^{z_{\rm H}}y^3e^{-3A}dy\int_{y_g}^{y}\frac{x}{e^Af}dx}}. \tag{2.23}$$

Finally, the potential can be solved from the eq. (2.16) as

$$V(z)=-3z^2ge^{-2A}\left[A''+3A'^2+\left(\frac{3g'}{2g}-\frac{6}{z}\right)A'-\frac{1}{z}\left(\frac{3g'}{2g}-\frac{4}{z}\right)+\frac{g''}{6g}\right]. \tag{2.24}$$

In summary, the analytic solutions of the equations of motion (2.13)–(2.16) are

$$\phi'(z)=\sqrt{-6\left(A''-A'^2+\frac{2}{z}A'\right)}, \tag{2.25}$$

$$A_t(z)=\sqrt{\frac{-1}{\int_0^{z_{\rm H}}y^3e^{-3A}dy\int_{y_g}^{y}\frac{x}{e^Af}dx}}\int_{z_{\rm H}}^{z}\frac{y}{e^Af}dy, \tag{2.26}$$

$$g(z)=1-\frac{\int_0^{z}y^3e^{-3A}dy\int_{y_g}^{y}\frac{x}{e^Af}dx}{\int_0^{z_{\rm H}}y^3e^{-3A}dy\int_{y_g}^{y}\frac{x}{e^Af}dx}, \tag{2.27}$$

$$V(z)=-3z^2ge^{-2A}\left[A''+3A'^2+\left(\frac{3g'}{2g}-\frac{6}{z}\right)A'-\frac{1}{z}\left(\frac{3g'}{2g}-\frac{4}{z}\right)+\frac{g''}{6g}\right], \tag{2.28}$$

where we have used the boundary conditions (2.17) and (2.18) to fix most of the integration constants except y_g. In fact, the only undetermined constant y_g is related to the chemical potential μ in the following way. We first expand the field $A_t(z)$ near the boundary at $z=0$,

$$A_t(0)=\sqrt{\frac{-1}{\int_0^{z_{\rm H}}y^3e^{-3A}dy\int_{y_g}^{y}\frac{x}{e^Af}dx}}\left(-\int_0^{z_{\rm H}}\frac{y}{e^Af}dy+\frac{1}{e^{A(0)}f(0)}z^2+\cdots\right). \tag{2.29}$$

Comparing the above expansion to eq. (2.19), we obtain the chemical potential μ in term of y_g as

$$\mu=-\sqrt{\frac{-1}{\int_0^{z_{\rm H}}y^3e^{-3A}dy\int_{y_g}^{y}\frac{x}{e^Af}dx}}\int_0^{z_{\rm H}}\frac{y}{e^Af}dy. \tag{2.30}$$

Using eq. (2.30), the integral constant y_g can be solved in term of the chemical potential μ once the explicit forms of $f(z)$ and $A(z)$ are given. Finally, putting the solution (2.25)–(2.28) into the constraint (2.12), it is straightforward to verify that the above solutions are satisfied with the constraint.

We note that the solutions (2.25)–(2.28) depend on two arbitrary functions, i.e. the gauge kinetic function $f(z)$ and the warped factor $A(z)$. Different choices of the functions $f(z)$ and $A(z)$ will give different physically allowed backgrounds. Thus we obtain a family of analytic solutions for the Einstein-Maxwell-dilaton system. We will use the freedom of choosing functions $f(z)$ and $A(z)$ to satisfy some extra important physical constraints.

JHEP11(2014)149

After solving the background, we consider the 5d probe vector field V whose equation of motion has been derived in (2.7),

$$\nabla_\mu \left[f(\phi) F_V^{\mu\nu} \right] = 0. \tag{2.31}$$

With the gauge $V_z = 0$, the equation of motion of the transverse vector field V_μ ($\partial^\mu V_\mu = 0$) in the above gravitational background becomes

$$\frac{1}{g}\nabla^2 V + V'' + \left(\frac{g'}{g} + \frac{f'}{f} + A' - \frac{1}{z} \right) V' = 0, \tag{2.32}$$

where the prime is the derivative respect to z. By expanding the vector field V for discrete values of 4d momentum $k_n = (\omega_n, \vec{p}_n)$,

$$V(x,z) = \sum_{k_n} e^{ik_n \cdot x} X \psi_n(z), \qquad X = \left(\frac{z}{e^A f g} \right)^{1/2}, \tag{2.33}$$

we bring the equation of motion (2.32) into the form of the Schrödinger equation,

$$-\psi_n'' + U(z)\psi_n = m_n^2(z)\psi_n, \tag{2.34}$$

with the potential function and the "energy dependent" mass,

$$U(z) = \frac{2X'^2}{X^2} - \frac{X''}{X}, \qquad m_n(z) = \sqrt{\frac{\omega_n^2}{g^2(z)} - \frac{\vec{p}_n^2}{g(z)}}. \tag{2.35}$$

In the limit of zero temperature and zero chemical potential, such that $g(z) \equiv 1$, we expect that the discrete spectrum of the vector mesons obeys the linear Regge trajectories. In this case, the above Schrödinger equation reduces to

$$-\psi_n'' + U(z)\psi_n = m_n^2 \psi_n, \tag{2.36}$$

where $m_n^2 = \omega_n^2 - \vec{p}_n^2$. To get the potential to be the form

$$U(z) = \frac{3}{4z^2} + c^2 z^2, \tag{2.37}$$

as in [9], we choose $f(z) = e^{\pm c z^2 - A(z)}$. The Schrödinger equations (2.36) with the above potential (2.37) have the discrete eigenvalues

$$m_n^2 = 4cn, \tag{2.38}$$

which is linear in the energy level n as we expect for the vector spectrum at zero temperature and zero density.

Once we fixed the gauge kinetic function $f(z) = e^{\pm c z^2 - A(z)}$, the eq. (2.30) can be solved to get the integration constant y_g in term of the chemical potential μ explicitly as

$$e^{c y_g^2} = \frac{\int_0^{z_H} y^3 e^{-3A} e^{cy^2} dy}{\int_0^{z_H} y^3 e^{-3A} dy} + \frac{\left(1 - e^{c z_H^2}\right)^2}{2c\mu^2 \int_0^{z_H} y^3 e^{-3A} dy}. \tag{2.39}$$

JHEP11(2014)149

Put the integration constant y_g back into the solution (2.25)–(2.28), we finally write down the completed solution as

$$\phi'(z) = \sqrt{-6\left(A'' - A'^2 + \frac{2}{z}A'\right)}, \tag{2.40}$$

$$A_t(z) = \mu\frac{e^{cz^2} - e^{cz_{\rm H}^2}}{1 - e^{cz_{\rm H}^2}}, \tag{2.41}$$

$$g(z) = 1 + \frac{1}{\int_0^{z_{\rm H}} y^3 e^{-3A} dy}\left[\frac{2c\mu^2}{\left(1 - e^{cz_{\rm H}^2}\right)^2}\begin{vmatrix} \int_0^{z_{\rm H}} y^3 e^{-3A} dy & \int_0^{z_{\rm H}} y^3 e^{-3A} e^{cy^2} dy \\ \int_{z_{\rm H}}^{z} y^3 e^{-3A} dy & \int_{z_{\rm H}}^{z} y^3 e^{-3A} e^{cy^2} dy \end{vmatrix} - \int_0^z y^3 e^{-3A} dy\right], \tag{2.42}$$

$$V(z) = -3z^2 g e^{-2A}\left[A'' + 3A'^2 + \left(\frac{3g'}{2g} - \frac{6}{z}\right)A' - \frac{1}{z}\left(\frac{3g'}{2g} - \frac{4}{z}\right) + \frac{g''}{6g}\right]. \tag{2.43}$$

Note that our final solution (2.40)–(2.43) still depends on the warped factor $A(z)$. The choice of $A(z)$ is arbitrary provided it satisfies the boundary condition (2.18).

3 Phase structure

To proceed, we need to choose a warped factor $A(z)$ first. In [19], a simple form of the warped factor has been studied,

$$A(z) = -\frac{c}{3}z^2 - bz^4. \tag{3.1}$$

The parameters $c \simeq 1.16\,GeV^2$ and $b \simeq 0.273\,GeV^4$ were determined by fitting the lowest two quarkonium states, $m_{J/\psi} = 3.096\,GeV$ and $m_{\psi'} = 3.685\,GeV$, as well as comparing the phase transition temperature at $\mu = 0$ to the lattice QCD simulation of $T_{HP} \simeq 0.6\,GeV$ in [20]. With these parameters, the authors of [19] argued that the system is to describe the heavy quarks with the deconfinement phase transition. However, in this work, we will consider another parameters regime of b and c to study the light quarks with the chiral symmetry breaking phase transition.

3.1 Meson spectrum

In this work, we consider the same form (3.1) of the warped factor $A(z)$ as in [19], but with the difference parameters regime of b and c. We will determine the parameter c first by fitting our mass formula (2.38) to the experimental data of the meson spectrum. In [19], we studied confinement/deconfinement phase transition in QCD for heavy quarks. The phase diagram we obtained for heavy quarks is quite different from the one for light quarks, which is consistent with the lattice QCD prediction. In this work, we are going to study the opposite situation, namely the phase diagram for light quarks, which is a more interested subject. Therefore, instead of fitting the quarkonium states made up of heavy quarks in [19], we now consider vector mesons made up of light quarks, specifically the $\rho(1^-)$ mesons. We take the experimental data of the lowest six excitations of $\rho(1^-)$ vector

JHEP11(2014)149

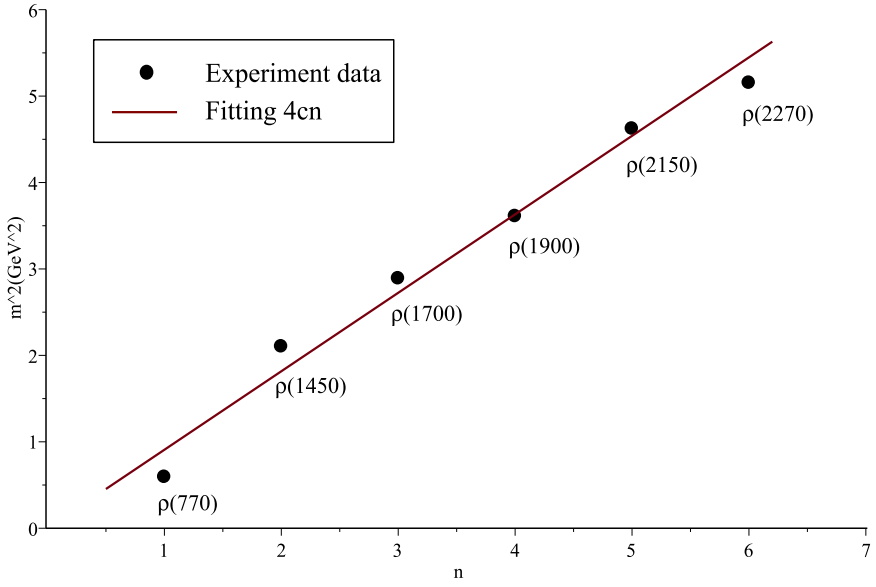

Figure 1. the squared masses of the lowest six excitations of $\rho(1^-)$ mesons versus their consecutive number n.

n	1	2	3	4	5	6
Experimental	0.77	1.45	1.70	1.90	2.15	2.27
Model fitting	0.95	1.35	1.65	1.90	2.13	2.34

Table 1. The mass specturm (in GeV) of the lower excitations of $\rho\,(1^{--})$ meson from PDG2007 [22] and their model fitting values...

mesons from PDG2007 [22], which are listed in table 1. To be more complete, beside the well confirmed three vector mesons $\rho\,(770)$, $\rho\,(1450)$ and $\rho\,(1700)$, we also include $\rho\,(1900)$ and $\rho\,(2150)$ as two confirmed mass resonances and $\rho\,(2270)$ as a yet confirmed mass resonance. From the data, we fit the parameter $c \simeq 0.227\,GeV^2$ in the mass formula (2.38) by using the standard χ^2 fit [23, 24]. Our model fitting values are also listed in table 1, which are consistent with the experimental data reasonably well. Figure 1 shows the squared masses of the lowest six excitations of $\rho\,(1^-)$ mesons versus their consecutive number n. The straight line is our model fitting $m_n^2 = 4cn$.

3.2 Black hole thermodynamics

Using the black hole solution we obtained in the previous section,

$$ds^2 = \frac{e^{2A(z)}}{z^2}\left[-g(z)dt^2 + \frac{dz^2}{g(z)} + d\vec{x}^2\right], \tag{3.2}$$

it is easy to calculate the Hawking-Bekenstein entropy

$$s = \frac{e^{3A(z_{\rm H})}}{4z_{\rm H}^3}, \tag{3.3}$$

JHEP11(2014)149

and the Hawking temperature

$$T=\frac{z_{\rm H}^3 e^{-3A(z_{\rm H})}}{4\pi\int_0^{z_{\rm H}} y^3 e^{-3A(y)}dy}\left[1-\frac{2c\mu^2\left(e^{cz_{\rm H}^2}\int_0^{z_{\rm H}} y^3 e^{-3A(y)}dy-\int_0^{z_{\rm H}} y^3 e^{-3A(y)}e^{cy^2}dy\right)}{\left(1-e^{cz_{\rm H}^2}\right)^2}\right]. \quad (3.4)$$

To continue, we need to fix the parameter b in the warped factor (3.1) for our black hole background.

In principle we could fix the parameter b by fitting the phase transition temperature $T_0\approx 170\,MeV$ at the vanishing chemical potential obtained from lattice QCD. However, it is well known that, for QCD with quark mass, the phase transition becomes a crossover at low chemical potential. There is no realizing order parameter to describe a crossover so that we can fit the order parameter to fix the parameter b. In this case, people usually define a quasi-transition temperature by looking at a rapid change for certain observable (as a quasi-order-parameter). In [25], the authors argued that the quasi-transition temperature for a crossover is not uniquely defined and therefore depends on the observable used to define it. Basically any observable that exhibits a non-differentiable behavior at the critical temperature (the temperature at which the phase transition becomes a crossover) can be used to define a quasi-transition temperature for a crossover. It is not surprised that the quasi-transition temperature might be different with the different observables used to define it. In this case, people use the transition region [26], in which different observable may have their characteristic points at different temperature values. Nevertheless, the purpose of this paper is not to discuss what the best way is to define the quasi-transition temperature for a crossover. We are going to simply choose an observable with appropriate property to define our quasi-transition temperature. The observable we will use to define the quasi-transition temperature for a crossover in this paper is the speed of sound because it is non-differentiable at the critical temperature and becomes a rapid change for a crossover at lower temperature. The speed of sound is defined as

$$c_s^2=\frac{\partial\ln T}{\partial\ln s}. \quad (3.5)$$

At $\mu=0$, the Hawking temperature (3.4) reduces to

$$T\left(z_{\rm H}\right)=\frac{z_{\rm H}^3 e^{-3A(z_{\rm H})}}{4\pi\int_0^{z_{\rm H}} y^3 e^{-3A(y)}dy}, \quad (3.6)$$

and the speed of sound can be calculated as

$$c_s^2=\frac{z_{\rm H}^4 e^{-3A(z_{\rm H})}}{3\left[1-z_{\rm H}A'\left(z_{\rm H}\right)\right]\int_0^{z_{\rm H}} y^3 e^{-3A(y)}dy}-1.$$

In figure 2, we plot the squared speed of sound v.s. temperature at vanishing chemical potential for several values of parameter b in the warped factor (3.1). We can see that, for each curve, there is a rapid change at a temperature around $150\sim 200\,MeV$, which we can use to define the quasi-transition temperature T_0 of the crossover at $\mu=0$. For different values of the parameter b, quasi-transition temperature T_0, i.e. the position of the minimum value, changes as shown in figure 2. By taking the commonly used value $T_0\approx 170\,MeV$, we can fix the parameter as $b=-6.25\times 10^{-4}\,GeV^4$.

JHEP11(2014)149

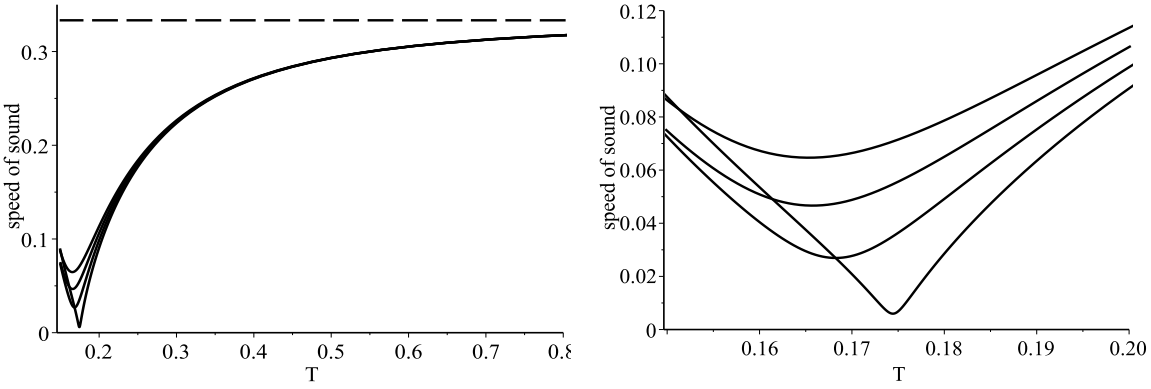

Figure 2. The squared speed of sound v.s. temperature at $\mu = 0$ for different values of parameter b. Curves from top to bottom correspond to $b = -0.0005, -0.0007, -0.0009, -0.0011\, GeV^4$. We enlarge a rectangle region in (a) into (b) to see the detailed structure. For different values of the parameter b, the corresponding quasi-transition temperature T_0, i.e. the position of the minimum value, changes.

3.3 Phase diagram

For different chemical potentials, the temperature dependence on the horizon $z_{\rm H}$ is showed in figure 3. For vanishing or small chemical potential $0 \leq \mu \leq \mu_c = 0.23148\, GeV$, the temperature decreases monotonously to zero; while for $\mu > \mu_c$, the temperature bends up and goes down again to zero. Therefore, for certain range, the same temperature corresponds to three different horizons as indicated in (b) of figure 3. This temperature behavior implicates that a phase transition happens at certain temperature for $\mu > \mu_c$.

To determine the thermodynamically stability, we plot specific heat C_V v.s. temperature T in figure 4, where the specific heat C_V is defined as

$$C_V = T\left(\frac{\partial s}{\partial T}\right)_{\mu}. \tag{3.7}$$

In the $C_V - T$ diagram, the negative value of the specific heat corresponds to the thermodynamically instability. For $0 \leq \mu \leq \mu_c$, the specific heat is always positive. $C_V > 0$ implies that the black hole with any temperature is thermodynamically stable. While for $\mu > \mu_c$, C_V could be negative for a range of T where the black hole is thermodynamically unstable. Thus one of the three horizons corresponding to the same temperature is thermodynamically unstable and the black hole would never take that state. However, there still left two horizons which are both thermodynamically stable and are possible realistic states. To determined which one is physically preferred out of the two thermodynamically stable states, we need to compare their free energies.

The first law of thermodynamics in a grand canonical ensemble can be written as,

$$F = U - Ts - \mu\rho, \tag{3.8}$$

JHEP11(2014)149

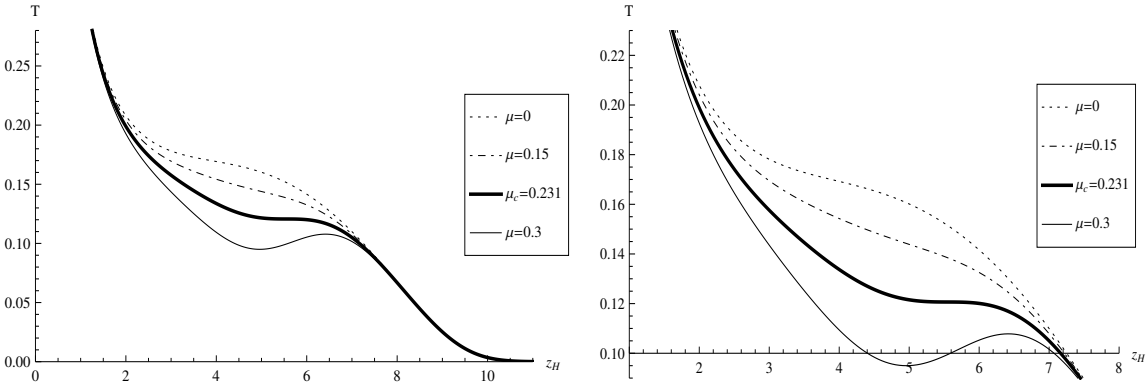

(a) **(b)**

Figure 3. The temperature v.s. horizon at different chemical potentials $\mu = 0, 0.15, 0.231, 0.3\,GeV$. We enlarge a rectangle region in (a) into (b) to see the detailed structure. For $0 < \mu < \mu_c$, the temperature decreases monotonously to zero; while for $\mu > \mu_c$, the temperature has a local minimum. At $\mu_c \simeq 0.231\,GeV$, the local minimum reduces to a inflection point.

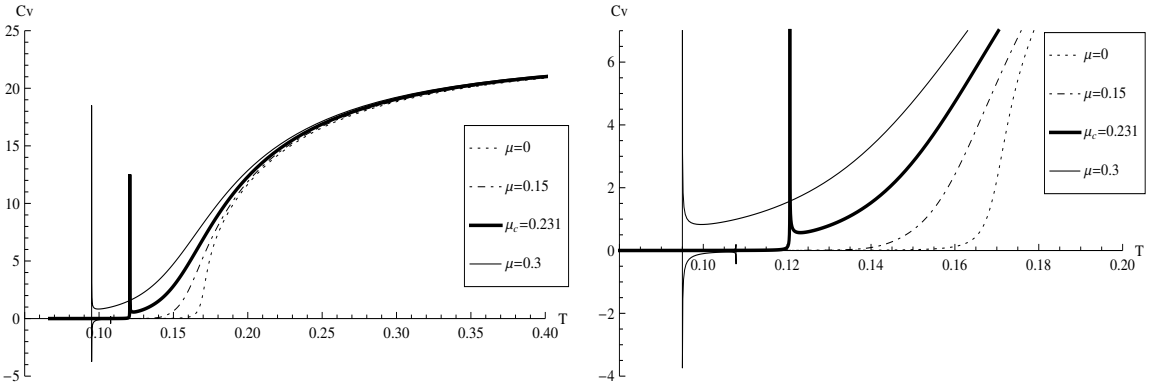

(a) **(b)**

Figure 4. The specific heat v.s. temperature at different chemical potentials $\mu = 0, 0.15, 0.231, 0.3\,GeV$. We enlarge a rectangle region in (a) into (b) to see the detailed structure. For $0 \leq \mu \leq \mu_c$, the specific heat is always positive, $C_V > 0$ implies that the black hole with any temperature is thermodynamically stable. While for $\mu > \mu_c$, C_V could be negative for a range of T where the black hole is thermodynamically unstable.

where U is the internal energy of the system and F is the corresponding free energy. Changes in the free energy of a system with constant volume are given by

$$dF = -sdT - \rho d\mu. \tag{3.9}$$

At fixed values of the chemical potential μ, the free energy can be evaluated by the integral [19, 27]

$$F = -\int sdT. \tag{3.10}$$

Directly integrating shows that the absolute value of the free energy goes to infinity and needs to be regularized. However, since we only care about the differences between the free

JHEP11(2014)149

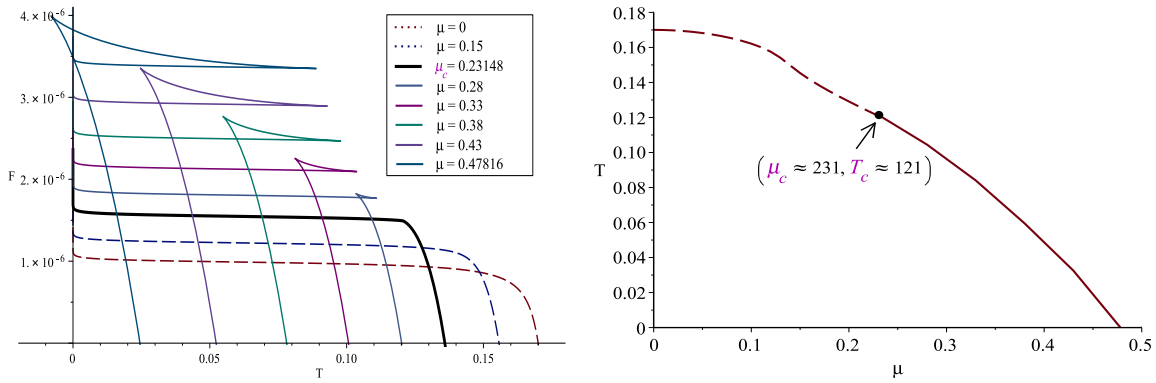

(a) **(b)**

Figure 5. The free energy v.s. temperature at different chemical potentials μ is plotted in (a) and the phase diagram in T and μ plane is plotted in (b). For $0 \leq \mu \leq \mu_c$, the free energies are single-valued and smooth, the system undergoes a crossover. While for $\mu > \mu_c$, the free energies become multi-valued and take swallow-tailed shapes with a first-order phase transition happens at the self-crossing point. At $\mu = \mu_c$, the free energy curve is single-valued but not smooth. A second-order phase transition happens at the non-smooth point $(\mu_c, T_c) \simeq (231\,MeV, 121\,MeV)$, which is the critical point where the phase transition mildens to a crossover.

energies, the absolute values of the free energy are not important for our analysis. Thus we can simply regularize the free energy by fixing the integration constant in the above integral (3.10). Considering the vanishing chemical potential case, we set the free energy at the quasi-transition temperature $T_0 \approx 170\,MeV$ to be zero. By requesting $F(T_0) = 0$ at $\mu = 0$, we finally are able to calculate the free energy as

$$F = \int_{z_{\rm H}}^{z_{\rm H}(T_0)} s \frac{dT}{dz_{\rm H}} dz_{\rm H}. \tag{3.11}$$

The free energy F v.s. temperature T and the phase diagram are plotted in figure 5.

As we expected, for $0 \leq \mu \leq \mu_c$, the free energies are always single-valued; while for $\mu > \mu_c$, the free energies become multi-valued and take swallow-tailed shapes. A first-order phase transition happens at the self-crossing point of each free energy curve with a fixed chemical potential. At $\mu = \mu_c$, the free energy curve is continues but not smooth. A second-order phase transition happens at the non-smooth point, which is the critical point where the phase transition mildens to a crossover.

3.4 Equations of state

Figure 6 plots the squared of speed of sound c_s^2 v.s. the temperature T for different chemical potentials.

For $0 < \mu < \mu_c$, the speed of sound behaves as a sharp but smooth crossover. At the critical point $\mu = \mu_c$, a second order phase transition happens where c_s^2 goes to 0 at the critical temperature T_c. For $\mu > \mu_c$, the squared of speed of sound becomes negative, i.e. the speed of sound is imaginary, for a range of temperature. The imaginary speed of sound indicates a Gregory-Laflamme instability [28, 29]. This is related to the general

JHEP11(2014)149

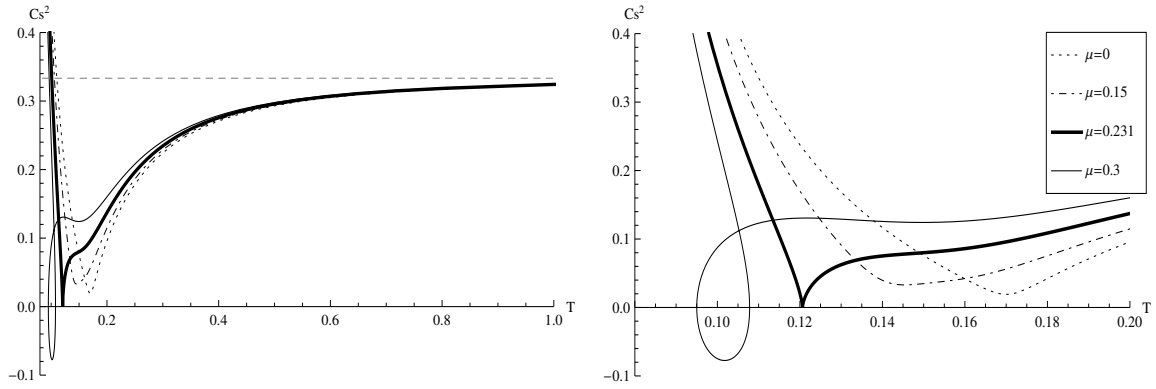

Figure 6. The squared speed of sound v.s. temperature at different chemical potentials $\mu = 0$, 0.15, 0.231, $0.3\,GeV$. We enlarge a rectangle region in (a) into (b) to see the detailed structure. For $0 < \mu < \mu_c$, the speed of sound behaves as a smooth crossover. At the critical point $\mu = \mu_c$, a second order phase transition happens where c_s^2 goes to 0 at the critical temperature T_c. For $\mu > \mu_c$, the squared of speed of sound undergoes a first order phase transition at the self-crossing point. At high temperature, c_s^2 approaches the conformal limit 1/3 as expected.

version of Gubser-Mitra conjecture [30–32], i.e. the dynamical stability of a horizon is equivalent to the thermodynamic stability. In our system, the negative specific heat implies thermodynamically unstable. While the imaginary speed of sound implies the amplitude of the fixed momentum sound wave would increase exponentially with time, reflecting the dynamical instability. Roughly speaking, $C_V < 0$ is equivalent to $c_s^2 < 0$ in our system. In all the case, c_s^2 approaches the conformal limit 1/3 at very high temperature as expected.

We plot equations of state for entropy in figure 7. For $0 < \mu < \mu_c$, the entropy is single-valued and there is no phase transition. For $\mu \geq \mu_c$, the entropy is multi-valued for a region of temperature which indicates a phase transition between high entropy and low entropy black holes. The similar phase behaviors have been discussed in [12] for a holographic QCD model with different values of parameters tuned by hand.

The pressure $p = -F$ and the energy $\epsilon = F + sT$ can be calculated from the free energy and are plotted in figure 8. We see that both pressure and energy increases with the chemical potential, that pushes the phase transition temperature to the smaller values for growing μ. Our results are consistent to the recent lattice results with finite chemical potential [33].

We finally plot the trace anomaly $\epsilon - 3p$ v.s. T in figure 9. With the growing chemical potential μ, the peak of trace anomaly decreases. From (b) in figure 9, we clearly see that, for $0 < \mu < \mu_c$, the trace anomaly is single-valued with finite slope through all the curve. For $\mu \geq \mu_c$, the slope of the trace anomaly becomes infinite at the certain temperature indicating a phase transition happened there.

4 Conclusion

In this paper, we studied a Einstein-Maxwell-dilaton system with a gauge kinetic function and a dilaton potential. We consistently solved the equations of motion for the system by

JHEP11(2014)149

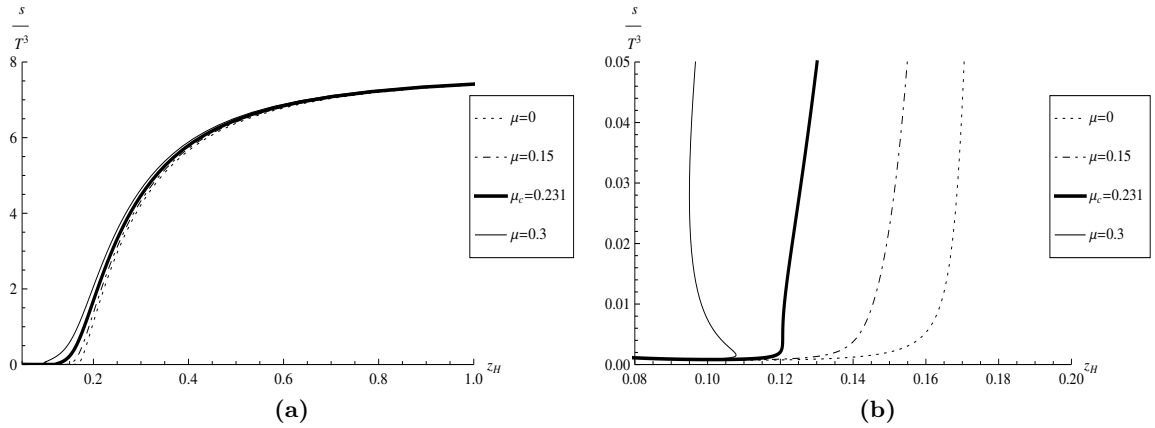

Figure 7. The entropy v.s. temperature at different chemical potentials $\mu = 0, 0.15, 0.231, 0.3\,GeV$. We enlarge a rectangle region in (a) into (b) to see the detailed structure. For $0 < \mu < \mu_c$, the entropy is single-valued and there is no phase transition. For $\mu \geq \mu_c$, the entropy is multi-valued for a region of temperature which indicates a phase transition between high entropy and low entropy black holes.

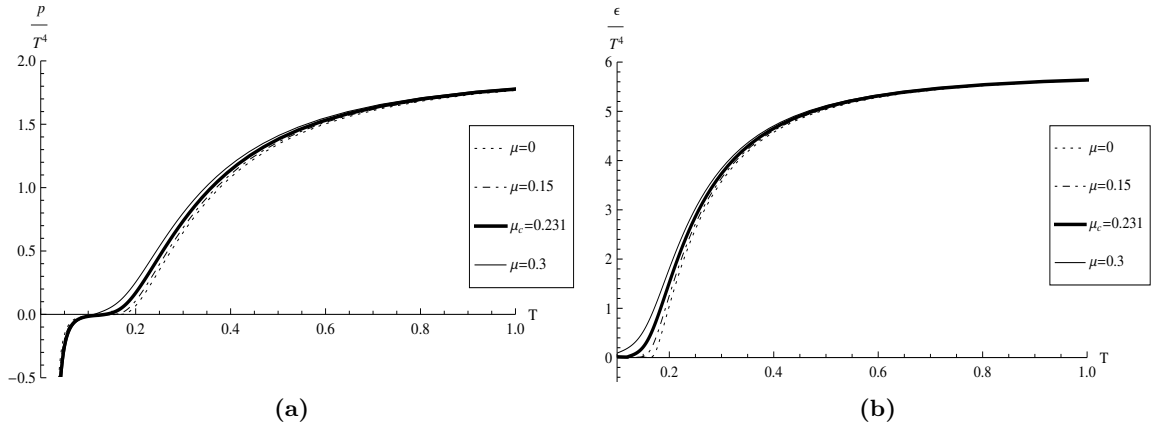

Figure 8. The equations of state at different chemical potentials $\mu = 0, 0.15, 0.231, 0.3\,GeV$. The pressure v.s. temperature is plotted in (a) and the energy v.s. temperature is plotted in (b).

the potential reconstruction method. A family of analytic black hole solutions is obtained. We then studied the thermodynamic properties of the black hole backgrounds. We computed the free energy to get the phase diagram of the black hole backgrounds. In its dual holographic QCD theory, we are able to realized the Regge trajectory of the vector mass spectrum by fixing the gauge kinetic function. We then calculated the equations of state in our holographic QCD model. We found that our dynamical model captures many properties in the realistic QCD. The most remarkable feature of our model is that, by changing the chemical potential, we are able to see the conversion from the phase transition to a crossover dynamically. We identified the critical point in our holographic QCD model and calculated its value with $(\mu_c, T_c) \simeq (0.231\,GeV, 0.121\,GeV)$. As the authors knowledge, our model is the first holographic QCD model which could both dynamically describe the

JHEP11(2014)149

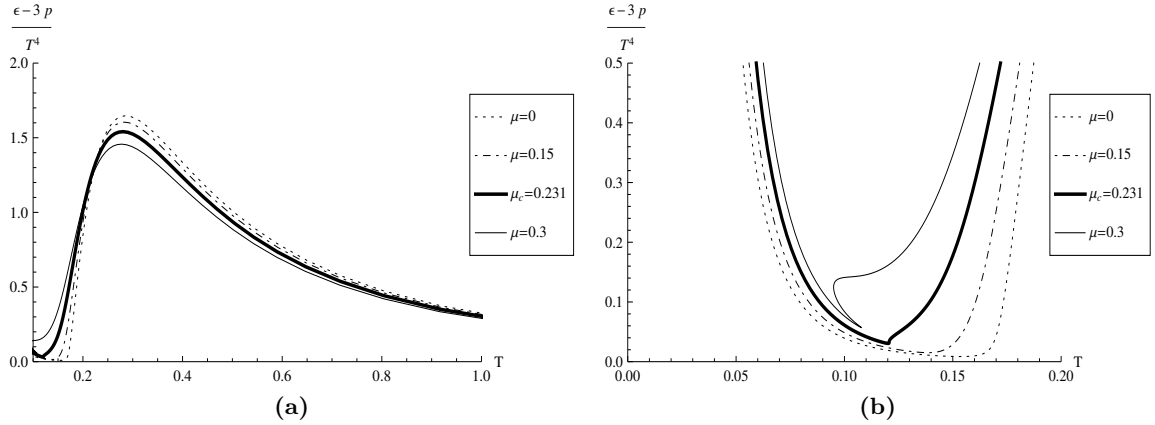

Figure 9. The trace anomaly v.s. temperature at different chemical potentials $\mu = 0,\ 0.15,\ 0.231,\ 0.3\,GeV$. We enlarge a rectangle region in (a) into (b) to see the detailed structure. For $0 < \mu < \mu_c$, the trace anomaly is single-valued with finite slope through all the curve. For $\mu \geq \mu_c$, the slope of the trace anomaly becomes infinite at the certain temperature indicating a phase transition happened there.

transformation from the phase transition to the crossover by changing the chemical potential and realize the linear Regge trajectory for meson spectrum. However, in this paper, we only studied the linear Regge trajectory for meson spectrum at zero temperature and zero density. At finite temperature or finite density, $g(z) \neq 1$, the masses of the vector mesons solved from the eq. (2.36) will depend on the temperature and density. For the case of small enough temperature or density, eq. (2.36) can be solved perturbatively to get the mass shift from the linear Regge trajectories [10, 34, 35]. For large temperature or density, the method of spectral functions is useful. It was showed that increasing temperature or density would modify the spectral function with the width of mass peak increasing, which implies the mesons become unstable. Eventually, the mass peak disappears above certain temperature/density indicating the mesons melt to free quarks. In addition, it was also showed that excited states melt at lower temperature/density respect to the ground state due to their peaks disappear earlier. The study of temperature and density dependent vector mass spectrum in our model is in progress.

There are many future directions are worth to be studied. For example, one can introduce a open string in the black hole background and compute the linear quark-antiquark potential and expectation value of Polyakov loop to incorporate the confinement-deconfinement phase transition. One can also compute the various transport coefficients like shear viscosity, bulk viscosity and so on. It is also interesting to compute the critical exponents of various physical quantities near the critical point. Some of these issues are in progress.

Acknowledgments

We would like to thank Mei Huang, Xiao-Ning Wu for useful discussions. This work is supported by the National Science Council (NSC 101-2112-M-009-005) and National Center for Theoretical Science, Taiwan.

JHEP11(2014)149

References

[1] O. Philipsen, *Lattice QCD at non-zero temperature and baryon density*, arXiv:1009.4089 [INSPIRE].

[2] J. Babington, J. Erdmenger, N.J. Evans, Z. Guralnik and I. Kirsch, *Chiral symmetry breaking and pions in nonsupersymmetric gauge/gravity duals*, *Phys. Rev.* **D 69** (2004) 066007 [hep-th/0306018] [INSPIRE].

[3] M. Kruczenski, D. Mateos, R.C. Myers and D.J. Winters, *Towards a holographic dual of large-N_c QCD*, *JHEP* **05** (2004) 041 [hep-th/0311270] [INSPIRE].

[4] M. Kruczenski, D. Mateos, R.C. Myers and D.J. Winters, *Meson spectroscopy in AdS/CFT with flavor*, *JHEP* **07** (2003) 049 [hep-th/0304032] [INSPIRE].

[5] S. Kobayashi, D. Mateos, S. Matsuura, R.C. Myers and R.M. Thomson, *Holographic phase transitions at finite baryon density*, *JHEP* **02** (2007) 016 [hep-th/0611099] [INSPIRE].

[6] T. Sakai and S. Sugimoto, *Low energy hadron physics in holographic QCD*, *Prog. Theor. Phys.* **113** (2005) 843 [hep-th/0412141] [INSPIRE].

[7] T. Sakai and S. Sugimoto, *More on a holographic dual of QCD*, *Prog. Theor. Phys.* **114** (2005) 1083 [hep-th/0507073] [INSPIRE].

[8] J. Erlich, E. Katz, D.T. Son and M.A. Stephanov, *QCD and a holographic model of hadrons*, *Phys. Rev. Lett.* **95** (2005) 261602 [hep-ph/0501128] [INSPIRE].

[9] A. Karch, E. Katz, D.T. Son and M.A. Stephanov, *Linear confinement and AdS/QCD*, *Phys. Rev.* **D 74** (2006) 015005 [hep-ph/0602229] [INSPIRE].

[10] B. Batell and T. Gherghetta, *Dynamical Soft-Wall AdS/QCD*, *Phys. Rev.* **D 78** (2008) 026002 [arXiv:0801.4383] [INSPIRE].

[11] W. de Paula, T. Frederico, H. Forkel and M. Beyer, *Dynamical AdS/QCD with area-law confinement and linear Regge trajectories*, *Phys. Rev.* **D 79** (2009) 075019 [arXiv:0806.3830] [INSPIRE].

[12] S.S. Gubser and A. Nellore, *Mimicking the QCD equation of state with a dual black hole*, *Phys. Rev.* **D 78** (2008) 086007 [arXiv:0804.0434] [INSPIRE].

[13] U. Gürsoy, E. Kiritsis, L. Mazzanti, G. Michalogiorgakis and F. Nitti, *Improved Holographic QCD*, *Lect. Notes Phys.* **828** (2011) 79 [arXiv:1006.5461] [INSPIRE].

[14] O. DeWolfe, S.S. Gubser and C. Rosen, *A holographic critical point*, *Phys. Rev.* **D 83** (2011) 086005 [arXiv:1012.1864] [INSPIRE].

[15] O. DeWolfe, S.S. Gubser and C. Rosen, *Dynamic critical phenomena at a holographic critical point*, *Phys. Rev.* **D 84** (2011) 126014 [arXiv:1108.2029] [INSPIRE].

[16] R.-G. Cai, S. He and D. Li, *A hQCD model and its phase diagram in Einstein-Maxwell-Dilaton system*, *JHEP* **03** (2012) 033 [arXiv:1201.0820] [INSPIRE].

JHEP11(2014)149

[17] D. Li, S. He, M. Huang and Q.-S. Yan, *Thermodynamics of deformed AdS_5 model with a positive/negative quadratic correction in graviton-dilaton system*, *JHEP* **09** (2011) 041 [arXiv:1103.5389] [INSPIRE].

[18] R.-G. Cai, S. Chakrabortty, S. He and L. Li, *Some aspects of QGP phase in a hQCD model*, *JHEP* **02** (2013) 068 [arXiv:1209.4512] [INSPIRE].

[19] S. He, S.-Y. Wu, Y. Yang and P.-H. Yuan, *Phase Structure in a Dynamical Soft-Wall Holographic QCD Model*, *JHEP* **04** (2013) 093 [arXiv:1301.0385] [INSPIRE].

[20] M. Fromm, J. Langelage, S. Lottini and O. Philipsen, *The QCD deconfinement transition for heavy quarks and all baryon chemical potentials*, *JHEP* **01** (2012) 042 [arXiv:1111.4953] [INSPIRE].

[21] P. Huovinen and P. Petreczky, *QCD Equation of State and Hadron Resonance Gas*, *Nucl. Phys.* **A 837** (2010) 26 [arXiv:0912.2541] [INSPIRE].

[22] Particle Data Group collaboration, W.M. Yao et al., *Review of Particle Physics*, *J. Phys.* **G 33** (2006) 1, and 2007 partial update for the 2008 edition [INSPIRE].

[23] M. Huang, S. He, , Q.-S. Yan and Y. Yang, *Confront Holographic QCD with Regge Trajectories*, *Eur. Phys. J.* **C 66** (2010) 187 [arXiv:0710.0988] [INSPIRE].

[24] M. Huang, Q.-S. Yan and Y. Yang, *Toward a more realistic holographic QCD model*, *Prog. Theor. Phys. Suppl.* **174** (2008) 334 [arXiv:0804.2731] [INSPIRE].

[25] J.M. Pawlowski and F. Rennecke, *Higher order quark-mesonic scattering processes and the phase structure of QCD*, arXiv:1403.1179 [INSPIRE].

[26] Wuppertal-Budapest collaboration, S. Borsányi et al., *Is there still any T_c mystery in lattice QCD? Results with physical masses in the continuum limit III*, *JHEP* **09** (2010) 073 [arXiv:1005.3508] [INSPIRE].

[27] U. Gürsoy, E. Kiritsis, L. Mazzanti and F. Nitti, *Holography and Thermodynamics of 5D Dilaton-gravity*, *JHEP* **05** (2009) 033 [arXiv:0812.0792] [INSPIRE].

[28] R. Gregory and R. Laflamme, *Black strings and p-branes are unstable*, *Phys. Rev. Lett.* **70** (1993) 2837 [hep-th/9301052] [INSPIRE].

[29] R. Gregory and R. Laflamme, *The Instability of charged black strings and p-branes*, *Nucl. Phys.* **B 428** (1994) 399 [hep-th/9404071] [INSPIRE].

[30] S.S. Gubser and I. Mitra, *Instability of charged black holes in Anti-de Sitter space*, hep-th/0009126 [INSPIRE].

[31] S.S. Gubser and I. Mitra, *The Evolution of unstable black holes in anti-de Sitter space*, *JHEP* **08** (2001) 018 [hep-th/0011127] [INSPIRE].

[32] H.S. Reall, *Classical and thermodynamic stability of black branes*, *Phys. Rev.* **D 64** (2001) 044005 [hep-th/0104071] [INSPIRE].

[33] S. Borsányi et al., *QCD equation of state at nonzero chemical potential: continuum results with physical quark masses at order μ^2*, *JHEP* **08** (2012) 053 [arXiv:1204.6710] [INSPIRE].

[34] L.-X. Cui, S. Takeuchi and Y.-L. Wu, *Thermal Mass Spectra of Vector and Axial-Vector Mesons in Predictive Soft-Wall AdS/QCD Model*, *JHEP* **04** (2012) 144 [arXiv:1112.5923] [INSPIRE].

[35] F. Giannuzzi, *Holographic vector mesons in a hot and dense medium*, *Nucl. Phys. Proc. Suppl.* **234** (2013) 309 [arXiv:1209.4198] [INSPIRE].

JHEP11(2014)149